

Behavior of mesogenic molecules deposited at the alumina-air interface: A deuteron NMR studyBoštjan Zalar,¹ Robert Blinc,¹ Slobodan Žumer,^{1,2} Tao Jin,³ and Daniele Finotello³¹*J. Stefan Institute, University of Ljubljana, Jamova 39, 1000 Ljubljana, Slovenia*²*Department of Physics, University of Ljubljana, Jadranska 19, 1000 Ljubljana, Slovenia*³*Department of Physics, Kent State University, Kent, Ohio 44242-0001*

(Received 7 December 2001; published 26 March 2002)

Thin molecular depositions of 4'-pentyl-4-cyanobiphenyl (5CB) mesogenic molecules are investigated via quadrupole-perturbed deuteron nuclear magnetic resonance (DNMR) spectroscopy. Uniform and controlled thickness molecular surface depositions are prepared on the inner cylindrical surfaces of Anopore membranes by the solvent-evaporation technique. As a result, 5CB molecules are found in two different configurations: a bulklike one with parallel axial arrangement, and a surface one with planar radial arrangement. If the 5CB surface coverage exceeds $c \approx 0.35$, only the bulk state is present. In the coverage range between 0.015 and 0.35, the bulklike state and the surface layer coexist, conforming to a typical dewetting scenario. Below $c \approx 0.015$, only the surface layer is present. The dilution of the surface deposition with decreasing coverage is manifested as an increase in the DNMR doublet frequency splitting. The surface orientational order parameter Q , the surface biaxiality η , and the diffusion coefficient D_S are determined from the DNMR spectral patterns obtained at different sample orientations in the external magnetic field. These angular patterns prove that in highly diluted surface depositions the molecules lie flat on the surface. However, they are not frozen and their molecular axes rapidly reorient on the DNMR measurement time scale, typically 10^{-4} s, while remaining confined to the surface. Simultaneously, molecules diffuse over the surface with a surface diffusion constant on the order of 10^{-11} m² s⁻¹. Such molecular diffusion is responsible for an effective biaxiality on the DNMR time scale. However, an inherent biaxiality cannot be completely ruled out and thus may play a minor role. The surface phase has a two-dimensional (2D) gas character with some (possible) indicators of 2D-liquid properties.

DOI: 10.1103/PhysRevE.65.041703

PACS number(s): 61.30.-v, 65.20.+w, 76.60.-k

I. INTRODUCTION

The study of lower-dimensionality systems has been a fascinating topic of research for several decades. The reasons for such interest are multiple. Simplistically, a film can be viewed as a two-dimensional (2D) analog of bulk. Films may be described in terms of elementary excitations that mirror in a lower dimension the excitations of the bulk system. However, films are usually much more complex because of additional variables that affect their properties as, for example, at a liquid-solid substrate or liquid-gas interfaces.

Perhaps the primary example, and undoubtedly one of the oldest and more extensively investigated low-dimensional systems, are superfluid helium films that are easily formed by adsorbing a known amount of helium onto any substrate. Near the superfluid transition, helium films differ in a fundamental way from bulk helium in the sense that they belong to a different universality class, the 2D-XY class [1]. As such, the film's critical behavior is drastically different from that of bulk helium. The heat capacity, which in 3D exhibits a nearly logarithmic singularity, is expected to be regular in 2D, namely, it has an essential singularity [2]. The superfluid density that in 3D vanishes with a 2/3 power law, in 2D has a discontinuity T_c [3]. The thermal conductivity that exhibits a power-law divergence in 3D, is exponentially divergent in 2D [4].

An additional reason for studying helium films is that they are easily formed and their thickness easily controlled. Consequently, by continuously adding a few moles of helium, a thicker film can be prepared and studies of physical param-

eters as a function of thickness easily performed. Therefore, it has been possible to study the superfluid transition in a purely 2D film, to a film thick enough that finite size effects are important, eventually crossing over to the bulk system [1].

Although there are many systems that can be studied in a "film" form, thermotropic liquid crystals (LC) are of particular interest due to their importance at the fundamental as well as applied levels. The ordering of liquid crystal molecules at the solid substrates is determined by a number of physical and chemical parameters, resulting in a rich variety of molecular arrangements at the solid-liquid interface as well as in the bulk liquid crystal phase above the interface. The behavior of the mesogen on lowering the dimensionality from 3D to 2D, i.e., on decreasing the thickness of the mesogenic layer gradually from a thick film with bulklike properties to a thin film, multilayer film, monolayer film, and finally to a submonolayer effective thickness molecular surface deposition is of particular interest, primarily in view of the stability of these structures. For thin 4'-pentyl-4-cyanobiphenyl (5CB) nematic films, spun cast onto silicon wafers, a spinodal-type dewetting into stable thick films was recently observed [5], and the driving mechanism explained in terms of the pseudo-Casimir structural force [6]. The dewetted regions were experimentally shown [7] to remain covered with a molecular film of microscopic dimensions, with an effective thickness of 1–3 molecular lengths. Similarly, the coexistence of a monolayer effective surface coverage and a bulklike nematic phase has been found for 5CB deposited on an alumina surface [8]. There seems to exist some universal

tendency for 5CB to exhibit monolayer-only wetting of solid substrates since in addition to silicon and alumina, this appears to be the case with glass and polyvinyl chloride substrates, as shown by some recent second-harmonic generation (SHG) experiments [9].

The question now open pertains to the physical nature of such a stable molecular deposition at the solid substrate-air interface. Does one deal with adsorbed molecules [10], a two-dimensional gas, or two-dimensional liquid? What is the respective orientational configuration of molecules? The existence of a monolayer, 2D liquid phase of nematogenic molecules at an air-water interface was demonstrated with Langmuir trough experiments [11] for a submonolayer effective thickness film (or more accurately, a molecular surface deposition) with an average area per molecule of about $A = 45 \text{ \AA}^2$, twice the value in the bulk phase [12]. A weak first-order phase transition from isotropic to polar orientation was also detected [13] on increasing the surface pressure. The $\vartheta = 62^\circ$ tilt of the 8CB polar group with respect to the interface normal calculated from SHG data, closely matches the $\vartheta = 68^\circ$ value obtained by only considering steric arguments that yield the optimal geometrical packing for 8CB molecules at the flat interface [11]. Surprisingly, similar tilt values are found by SHG experiments with nonsmectic 5CB deposited on solid substrates [9], again supporting the steric interactions-dominated interface ordering.

An estimate of the tilt in a monolayer 5CB deposition on alumina can be made from deuteron nuclear magnetic resonance (DNMR) measurements [8]. Using the definition of the orientational order parameter $Q = \overline{P_2(\cos \vartheta)}$, one can assume that all the molecules are tilted with respect to the surface normal and precess on the surface of the cone around the normal. One finds $\vartheta = \arccos[(1 + 2Q)/3]^{1/2}$, yielding $\vartheta \approx 61^\circ$ for $Q \approx -0.14$. This value of the orientational order is obtained whenever the surface deposition component coexists with a bulk phase [8]. Taking into account similar tilt values, this situation closely resembles the coexistence of a monolayer liquid phase with a thicker film as found in Ref. [11]. The solvent evaporation technique [8] made it possible to prepare molecular films with effective thickness far below a monolayer size in a controllable way. In other words, thin molecular depositions with well defined and variable area per molecule can be formed on a solid surface. Combining this fact with the distinctive DNMR ability of probing the molecular orientational order, the interplay between the particle density and their orientational order in a 2D system can be investigated.

A difficulty of the DNMR technique, namely, the need of a minimum number of deuterated molecules, is overcome by using porous hosts with high surface to volume ratios. In addition, if the topology of the surface is well defined, the DNMR spectral patterns can easily be interpreted; Anopore membranes [14] satisfy both criteria. By changing the amount of nematogenic molecules deposited on the Anopore internal walls, thus covering a certain size area, one effectively alters the surface molecular density, equivalently, the area per molecule A . This corresponds to changing the surface pressure of a molecular film at the liquid-air interface

using the Langmuir trough; here, the film is formed at a solid-air interface.

In most experimental investigations of surface ordering, the order at the surface is not probed directly, rather, it is deduced from changes in the behavior of the bulk phase, attributed to the influence of the surface. A standard approach is to calculate the equilibrium director configuration using the Landau-de Gennes free energy formalism for a bulk state with the inclusion of surface terms [15,16] and taking into account plausible boundary conditions. These can be, however, complex and may require a detailed knowledge of the surface topology and molecular anchoring. Different scenarios for molecular arrangement at the surface can lead to indistinguishable differences in the experimental response, thus making the reverse process of resolving between different surface configurations from a bulklike response, a somewhat tedious and at times inaccurate task. In spite of that, substantial progress made in recent years has yielded a quantitative characterization of physical parameters such as anchoring energy and surface orientational order parameter [14,17,18], particularly, in view of the atomic-scale interface morphology of the surface that can be manipulated by rubbing, grating, or surface treatment with surfactants. Still, for reasons given above, the direct detection of molecular ordering at a surface would be of great importance. It is of course rather difficult, whenever bulk is present, to design an experiment where one would be exclusively probing the molecules at the surface. In the case of optical experiments, it is the large birefringence of the bulk that makes it difficult [19], whereas the molecular diffusion between bulk and surface is the drawback in DNMR experiments, since it blends the “surface” and the “bulk” contributions in the NMR response [20]. The alternative approach is to look at ultrathin mesogenic film with just a “surface” phase. There are two problems that arise in this case. First, the surface-induced order in such a configuration may be considerably different from the one found when bulk is present; this is due to finite size effects and due to two (possibly even competing) boundary conditions-imposing media: the solid substrate on one side and gas (air) on the other side of the sandwiched thin LC film. Second, resolving the contributions of such a 2D structure may not be feasible in a planar geometry. In particular, 10^{18} molecules are typically needed to accumulate an observable DNMR signal in one hour. With an average area $A = 45 \text{ \AA}^2$ per molecule in a diluted molecular 2D deposition [11], more than 0.5 m^2 of substrate are required, an amount not easy to fit into a typical NMR probe head. The sensitivity problem can be solved by using porous solid hosts [21], preferably ones with well-defined geometry such as Nuclepore [22] or Anopore [14]. Thin-film depositions of LC molecules on large diameter cylindrical noninterconnected pores do not suffer from elastic deformations introduced by geometrical constraints since the curvature of the surface in the pores is small with respect to molecular dimensions; we are effectively dealing with a quasiplanar geometry.

In this paper we present a DNMR method to directly investigate the orientational behavior in ultrathin layers of mesogenic molecules, formed on alumina surface. We show how these submonolayer (effective) thickness molecular

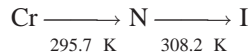
depositions can be prepared on the inner walls of the porous host. Coverages with different average area per molecule A can be formed in a reproducible manner and the molecular orientational ordering studied over a wide range of A spanning from close packed monolayer structures resembling liquidlike behavior in 2D, down to highly diluted depositions of molecules lying flat on the substrate surface. By taking advantage of a well-characterized nanoscopic geometry, we try to determine the properties of a thin molecular deposition, an approach opposite to that used in other NMR studies of the surface topology [23].

This paper offers an extension of the preliminary study presented in Ref. [8], with an in depth discussion of the measurements method and its potential in probing physical parameters such as orientational order parameter and the surface diffusion constant in ultrathin films via DNMR. The paper is organized in the following manner. Section II describes the materials used in the preparation of submonolayer effective thickness molecular depositions. An overview of director configurations found when Anopore are completely filled with a LC is given in Sec. III. Knowledge of these structures is later used to propose possible orientational configurations for ultrathin films. The DNMR experimental technique and its application to LC materials confined to a cylindrical geometry is discussed in Sec. IV. There, theoretical spectral line shapes are calculated for the general case of biaxial orientational ordering of molecules on cylindrical surfaces. The impact of molecular diffusion along the solid surface is treated in Sec. V. The resulting motionally averaged spectra are calculated and compared with the static ones of Sec. IV. Experimental results are given in Sec. VI, together with a thorough discussion. Section VII presents our conclusions.

II. MATERIALS

Anopore, commercially available membranes normally used in filtration applications, are made of chemically pure alumina (Al_2O_3). They have open, parallel cylindrical channels of diameter $d_0 = 2r_0 = 0.2 \mu\text{m}$ that extend through the entire $h_0 = 60 \mu\text{m}$ thickness of the membrane. The estimated porosity p_0 is about 40%, yielding a specific area $\sigma = S_{\text{inner}}/V = 2p_0/r_0$ of $8000 \text{ mm}^2/\text{mm}^3$ of Anopore material.

The liquid crystal material used in the study is the αd_2 -deuterated nematogenic 5CB (molecular mass $M_{5\text{CB}} = 251 \text{ g/mol}$) with the phase transition sequence



on heating. On cooling, the transition from the isotropic into the nematic phase occurs at the same temperature, $T_{\text{NI}} = 308.2 \text{ K}$, whereas the crystallization temperature is shifted down to about $273\text{--}277 \text{ K}$. On deuteration, neither chemical nor physical macroscopic properties of the material exhibit any notable changes.

Anopore were treated with 5CB by the solvent-evaporation technique. The basic idea is to dissolve the LC material in a solvent, soak the Anopore membranes in the

solution and let the solvent evaporate. In this way one is left with a deposition of LC molecules on the inner, cylindrical surfaces of the solid host. In our experiments, methanol was used as the solvent. The area S_{outer} of the outer, flat surface joining the openings of the cylindrical channels, is related to the inner surface area S_{inner} via $S_{\text{outer}} = S_{\text{inner}}r_0(1-p_0)/p_0h_0$. Using the above parameters one finds $S_{\text{outer}} = 0.025 S_{\text{inner}}$. Any signal originating from the outer surface can, therefore, be disregarded; the main contribution originates from the inner walls.

The effective thickness of the molecular deposition depends on the concentration of 5CB in the solution. Let us assume that a constant thickness film is formed. The concentration needed to form a film with an effective thickness d_{eff} is roughly given by

$$c = \left\{ 1 + \lambda \frac{(r_0 - d_{\text{eff}})^2}{2r_0d_{\text{eff}} - d_{\text{eff}}^2} \right\}^{-1}, \quad (1)$$

with $\lambda = \rho_{5\text{CB}}/\rho_{\text{CH}_3\text{OH}} \approx 1$ denoting the ratio of the 5CB and methanol mass densities, respectively. We have also assumed an ideal mixing of the two components (the volume is preserved on mixing). c , the surface coverage parameter thus also represents the 5CB pore-filling factor. A monolayer surface deposition, presumably equivalent to one 5CB molecular length ($l = 20 \text{ \AA}$) effective thickness, is, therefore, formed from a $c(d_{\text{eff}} = l) = c_l = 0.04$ solution. For ultrathin films, a more appropriate quantity than d_{eff} for the characterization of the surface coverage is the area per molecule A , which is related to c via

$$A = \left(1 + \lambda \frac{1-c}{c} \right) \frac{2M_{5\text{CB}}}{r_0N_A\rho_{5\text{CB}}} \approx \frac{0.84 \text{ \AA}^2}{c} \quad (2)$$

with N_A the Avogadro number. At the air-water surface, a 5CB monolayer resembling 2D-liquid phase is found for $48 \text{ \AA}^2 > A > 41 \text{ \AA}^2$ [11], and one may expect a similar behavior at the alumina-air interface. Inserting these values above yields $c_1 \approx 0.018$, or, a factor of 2 smaller than c_l . This discrepancy is understandable since in a monolayer the molecules are effectively tilted away from the surface normal. Consequently, the effective layer thickness is smaller than one molecular length, a fact that was ignored when calculating c_l .

The liquid crystal-solvent solutions were prepared starting with 5CB ($c = 1$) and adding methanol. In each step, one part of the solution was put aside to be used for the treatment of Anopore, whereas the rest was used for further dilution, so that a set of 5CB solutions with decreasing c was prepared. The most diluted sample had $c_{\text{min}} = 0.001$. Below $c = c_1$, where, according to conclusions drawn in the preceding paragraph, the transitional phenomena from a 2D liquid into a 2D gas phase are to be expected, the concentration of solution in each step was reduced in much smaller intervals in order to cover the $c_1 > c > c_{\text{min}}$ range more densely.

The collection of solutions was subsequently used to prepare a set of 5CB-treated Anopore with different area per molecule coverages, up to $A_{\text{max}} = 830 \text{ \AA}^2$ for c_{min} [Eq. (2)].

Anopore were cut to 4 mm×25 mm strips, each having a volume of $V_0=6\text{ mm}^3$. Typically 20 of them were used for the preparation of a sample from one solution, providing for a total of $S_{\text{inner}}=20\sigma V_0\approx 1\text{ m}^2$ available surface. This coverage corresponds to $N_{\text{min}}=2S_{\text{inner}}/A_{\text{max}}\approx 2.5\times 10^{17}$ deuteron nuclei for the sample with the lowest surface coverage, an amount still detectable in DNMR experiments.

III. 5CB ORIENTATIONAL ORDER IN ANOPORE

A. Full Anopore

In full Anopore, many different director configurations can be found in the nematic phase depending on the relative strength of surface interactions, elastic forces, and external fields. In the $\mathbf{B}_0=9\text{ T}$ magnetic field, used in our DNMR experiments, the magnetic coherence length is about 1 μm [14] and considerably exceeds the Anopore confinement size of 0.2 μm . External fields are, therefore, not expected to alter the director configuration. Elastic forces are introduced by geometrical constraints, i.e., the curvature of the surface. In nontreated Anopore completely filled with 5CB, the director configuration is parallel axial [14]. Neglecting surface effects, the axial alignment is energetically most favorable since such a spatially homogeneous structure demands no elastic energy. But as soon as surface energy terms become important, it is sometimes necessary to increase the elastic energy in order to minimize the surface contribution. This is the case with treated cavity walls where spatially inhomogeneous structures such as planar polar are found [14]. Also, a 5CB molecule in a submonolayer effective thickness film sees the surface of an $r_0=100\text{ nm}$ cylinder as flat. Consequently, in a thin-film LC molecular deposition with spatially homogeneous director field it is then the surface interactions and the geometrical packing of molecules that determines the molecular order.

B. Partially filled Anopore

Let us now inspect possible molecular configurations in a 2D film. We shall assume that cavity walls are smooth, with no grooves or scratches on the order of the 5CB molecular size. At the very surface, the inversion symmetry of the bulk nematic phase is lost, since it is the hydrophilic polar cyan head group that attaches to the surface [11]. In an ideal case one can expect that at extremely low coverages, equivalently, high A , where the molecules do not feel each other, their long axes lie flat on the surface [24]. At zero T they are adsorbed, frozen to the surface, and point in different directions with no long range orientational order, a situation typical for a frozen-in 2D molecular gas. On increasing T , dynamic modes begin to appear: reorientations about the long axis (including internal molecular conformations) [Fig. 1(a)], tumbling about the ‘‘C=N pivot’’ (the point at which the C=N group is attached to the solid surface) [Fig. 1(b)] and diffusionlike translational motion of the molecule, or equivalently, of the C=N pivot, along the surface [Fig. 1(c)]. We shall denote the corresponding correlation times as τ_R , τ_ζ , and τ_D , respectively. Explicitly, τ_R measures the time needed for a 2π reorientation about the long molecular axis

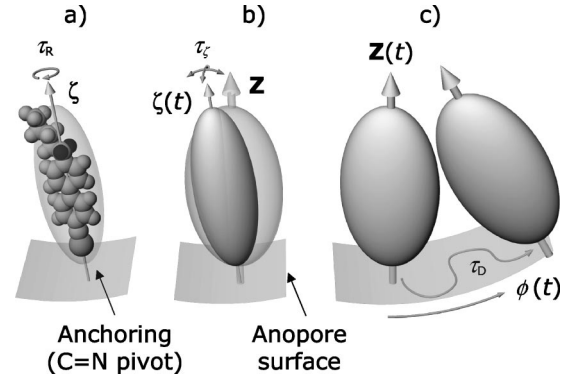


FIG. 1. A schematic picture of 5CB molecular dynamics: reorientations about the long molecular axis ζ with the correlation time τ_R (a), orientational fluctuations of ζ with the correlation time τ_ζ (b), and the surface diffusion, characterized with $\tau_D\propto D_S^{-1}$ (c). \mathbf{Z} is the largest eigenvalue (Q) eigenaxis of the orientational order parameter tensor and ϕ the angular coordinate of the molecule. Deuteration sites in the molecule are shown in dark color.

ζ , τ_ζ is the time scale of the orientational fluctuations (tumbling of the long axis), whereas $\tau_D=L^2/4D_S$ measures the time spent by a molecule while diffusing over a distance L on a surface. D_S is the surface diffusion constant for this process. In the bulk nematic phase of 5CB, the experimentally determined values at room T were $\tau_R\approx 10^{-9}\text{ s}$, $\tau_\zeta\approx 10^{-8}\text{ s}$ [25], and $D_S\approx 10^{-11}\text{ m}^2\text{ s}^{-1}$ [26]. The latter yields $\tau_D=10^{-7}\text{ s}$ for $L=l$, i.e., for displacements of the order of one molecular length. In what follows, we will assume that the rotational diffusion characterized by τ_R is always fast compared to the other two processes, i.e., $\tau_R\ll\tau_\zeta,\tau_D$, and consequently, that each molecule can be regarded as a solid, cylindrically symmetric rod, pinned to the surface with its C=N end. The two processes of our interest are, therefore, the orientational fluctuations and the translational diffusion over the surface, respectively. At this point, we will concentrate only on the former.

Let us choose a local coordinate system \mathbf{xyz} with its \mathbf{z} axis normal to the surface and \mathbf{y} axis lying on the surface and pointing along the cylindrical cavity symmetry axis [Fig. 2(c)]. ϑ and ϑ are the phase and azimuth angles, respectively, describing the instantaneous orientation $\zeta(t)$ of the long molecular axis in the \mathbf{xyz} frame. The static properties of the local orientational order are described by the orientational probability distribution function

$$W(\cos\vartheta,\varphi)=\sum_{l=0}^{\infty}a_lP_l(\cos\vartheta)+\sum_{l=0,m=1}^{\infty,l}(s_{lm}\sin m\varphi+c_{lm}\cos m\varphi)P_{lm}(\cos\vartheta). \quad (3)$$

$P_l(\cos\vartheta)$ and $P_{lm}(\cos\vartheta)$ are the Legendre and associated Legendre polynomials, respectively. The expansion coefficients $\{a_l,s_{lm},c_{lm}\}$ uniquely determine $W(\cos\vartheta,\varphi)$. In bulk systems, there is no polar ordering, i.e., there are no odd l terms due to inversion symmetry $W(\cos\vartheta,\varphi)=W(\cos(\pi-\vartheta),\varphi+\pi)$. The latter is broken at surfaces which induce polar ordering [27] as it is the case here.

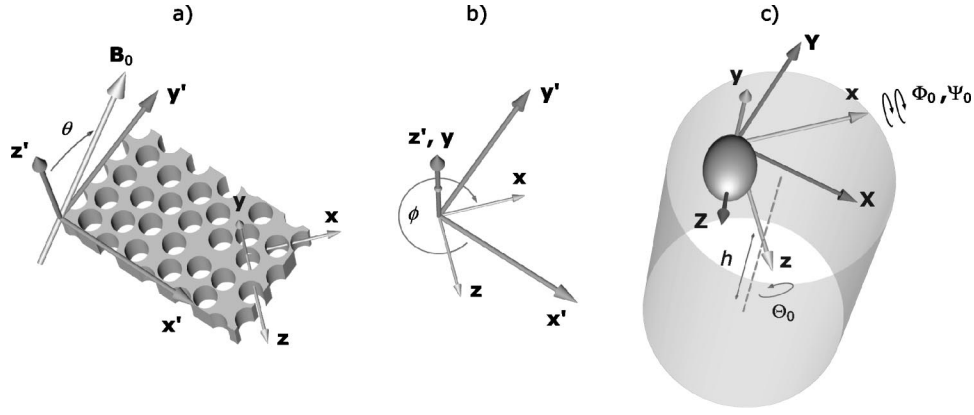


FIG. 2. Coordinate frames used in the description of molecular orientational ordering. The “crystal” frame $\mathbf{x}'\mathbf{y}'\mathbf{z}'$, fixed to the Anopore strip is shown in (a), and its transformation into the local frame \mathbf{xyz} in (b). The orientation of the local frame with respect to the orientational order parameter eigensystem \mathbf{XYZ} is presented in (c). The Euler rotation $R_{xyz \rightarrow XYZ}(\Psi_0, \Theta_0, \Phi_0)$ of \mathbf{xyz} into \mathbf{XYZ} is constructed from three consecutive rotations: Φ_0 rotation about \mathbf{x} , Θ_0 rotation about \mathbf{z} , and Ψ_0 rotation about \mathbf{x} .

IV. DEUTERON QUADRUPOLE-PERTURBED NMR

A. DNMR and the surface orientational order parameter tensor

The quadrupole-perturbed NMR spectrum of an α deuteron in a frozen-in 5CB molecule consists of two resonance lines (denoted by the \pm sign) that are shifted in frequency

$$\delta\nu^\pm = \pm \frac{3}{4} \nu_q P_2(\cos \gamma') \quad (4)$$

from the deuteron Larmor frequency ν_L . ν_q is the quadrupole coupling constant, which is proportional to the largest eigenvalue $V_{\xi\xi}$ of the cylindrically symmetric [28] electric field gradient (EFG) tensor at the deuteron site. The axis of symmetry points along the direction ξ of the C-D bond. It is γ' that measures the angle between ξ and the external magnetic field \mathbf{B}_0 . In 5CB mesophases, reorientations of ξ about the long molecular axis ζ are unbiased and fast on the DNMR time scale $\tau_{\text{DNMR}} \approx \nu_q^{-1} \approx 5 \times 10^{-6}$ s. This has two consequences: first, the two α deuterons become indistinguishable in the DNMR spectrum, and second, their respective EFG tensors average out into a cylindrically symmetric one with symmetry axis pointing along ζ , with $V_{\zeta\zeta} = V_{\xi\xi} P_2(\cos \beta)$. Here β is the constant angle between ζ and ξ . In an ideal tetrahedronlike configuration of the C-D bonds, the one we shall assume in what follows, one has $\beta = \arccos(-1/3) = 109.5^\circ$ and $V_{\zeta\zeta} = -V_{\xi\xi}/3$. Then, taking into account the proportionalities $\nu_q \propto V_{\xi\xi}$ and $\bar{\nu}_q \propto V_{\zeta\zeta}$, $\bar{\nu}_q = \nu_q P_2(\cos \beta) = \nu_q/3$ is satisfied and the averaged frequency shift is

$$\overline{\delta\nu^\pm} = \pm \frac{1}{4} \nu_q P_2(\cos \gamma), \quad (5)$$

where $\gamma = \angle(\zeta, \mathbf{B}_0)$ denotes the angle between the effectively rodlike molecule and the magnetic field. The ratio of experimentally determined values $\nu_q \approx 180$ kHz [28] and $\bar{\nu}_q \approx 60$ kHz [29] amounts to $\bar{\nu}_q/\nu_q \approx 1/3$, thus supporting the above assumption. In order to relate the DNMR frequency

shift to the molecular orientational order, let us write ζ and $\mathbf{b} = \mathbf{B}_0/B_0$ in the local frame \mathbf{xyz} coordinates,

$$\zeta = (\zeta_x, \zeta_y, \zeta_z) = (\sin \vartheta \cos \varphi, \sin \vartheta \sin \varphi, \cos \vartheta), \quad (6a)$$

$$\mathbf{b} = (b_x, b_y, b_z) = (\sin \vartheta_b \cos \varphi_b, \sin \vartheta_b \sin \varphi_b, \cos \vartheta_b). \quad (6b)$$

One can then recast Eq. (5), averaged over orientational fluctuations of ζ , into

$$\begin{aligned} \nu^\pm &= \pm \frac{1}{8} \nu_q [3 \langle (\zeta \cdot \mathbf{b})^2 \rangle - 1] \\ &= \pm \frac{1}{8} \nu_q \left[3 \sum_{\alpha, \beta} b_\alpha b_\beta \langle \zeta_\alpha \zeta_\beta \rangle - 1 \right], \end{aligned} \quad (7)$$

with $\alpha, \beta = x, y, z$ and $\nu^\pm = \langle \overline{\delta\nu} \rangle^\pm$. Here $\langle \cdot \cdot \cdot \rangle$ stands for the average over $W(\cos \vartheta, \varphi)$. $\langle \zeta_\alpha \zeta_\beta \rangle$ are the components of the second rank tensor. These can be expressed as linear combinations of the $l=2$ coefficients of $W(\cos \vartheta, \varphi)$ [Eq. (3)], so that ν^\pm only depends on the $l=2$ terms of the molecular orientational distribution. Hence the polar order, described formally with the $l=1$ coefficients, cannot be probed by DNMR line-shape measurement.

Since $\sum_\alpha \zeta_\alpha^2 = 1$ is always satisfied, the redefined quantities $Q_{\alpha\beta} = (3 \langle \zeta_\alpha \zeta_\beta \rangle - \delta_{\alpha\beta})/2$ constitute a traceless second rank tensor \underline{Q} , equivalent to the classical orientational order parameter of a bulk LC phase [30]. Its largest eigenvalue $Q = Q_{ZZ}$ corresponds to the nematic order parameter, whereas $\eta = (Q_{XX} - Q_{YY})/Q_{ZZ}$, the biaxiality parameter, measures the deviation from uniaxial symmetry around the \mathbf{Z} eigenaxis. In its eigensystem \mathbf{XYZ} , \underline{Q} is completely specified by Q and η since $Q_{XX} + Q_{YY} + Q_{ZZ} = 0$. ν^\pm is a scalar quantity, i.e., its value must not depend on the coordinate frame where the components of \mathbf{b} and \underline{Q} are written out. As a result,

$$\begin{aligned}\nu^\pm &= \pm \frac{1}{4} \nu_q \sum_{\alpha,\beta} b_\alpha b_\beta Q_{\alpha\beta} = \pm \frac{1}{4} \nu_q \sum_\lambda b_\lambda^2 Q_{\lambda\lambda} \\ &= \pm \frac{1}{8} \nu_q Q [3b_Z^2 - 1 + \eta(b_X^2 - b_Y^2)],\end{aligned}\quad (8)$$

with $\lambda = X, Y, Z$. Introducing Θ and Φ , the tilt and the phase angle, respectively, of the external magnetic field $\mathbf{b} = (b_X, b_Y, b_Z) = (\sin \Theta \cos \Phi, \sin \Theta \sin \Phi, \cos \Theta)$ expressed in the \mathbf{XYZ} frame, the eigenframe of the orientational order parameter \underline{Q} , Eq. (8) becomes [31]

$$\nu^\pm = \pm \frac{1}{8} \nu_q Q [3 \cos^2 \Theta - 1 + \eta \sin^2 \Theta \cos 2\Phi]. \quad (9)$$

Now, it is necessary to relate the \underline{Q} eigensystem to the ‘‘crystal’’ frame $\mathbf{x}'\mathbf{y}'\mathbf{z}'$ that is fixed to the Anopore strip [Fig. 2(a)], with its \mathbf{z}' axis pointing along the symmetry axis of the cylindrical cavities. To that end, let us describe the orientation of the sample with θ , the angle between \mathbf{z}' and the magnetic field \mathbf{B}_0 ; hence $\mathbf{b}_{x'y'z'} = (b_{x'}, b_{y'}, b_{z'}) = (0, \sin \theta, \cos \theta)$. The magnetic field vectors \mathbf{b}_{XYZ} and $\mathbf{b}_{x'y'z'}$, expressed in the ordering tensor frame and in the crystal frame, respectively, are related via

$$\begin{aligned}\mathbf{b}_{XYZ} &= R_{xyz \rightarrow XYZ}^{-1}(\Psi_0, \Theta_0, \Phi_0) \\ &\times R_{x'y'z' \rightarrow xyz}^{-1}(0, \pi/2, -\phi) \mathbf{b}_{x'y'z'},\end{aligned}\quad (10)$$

where $R_{xyz \rightarrow XYZ}$ represents the Euler rotation [32] of the local coordinate system \mathbf{xyz} into the ordering tensor eigensystem \mathbf{XYZ} , whereas $R_{x'y'z' \rightarrow xyz}$ is the respective rotation of the ‘‘crystal’’ system $\mathbf{x}'\mathbf{y}'\mathbf{z}'$ into the local system \mathbf{xyz} . The position of the local coordinate system in a cavity is given by its azimuthal angle $\phi \in [0, 2\pi]$ and the altitude coordinate h [Fig. 2(c)]. The translation of the molecule on the surface in parallel with \mathbf{z}' , i.e., the variation of h , does not change its orientation with respect to the magnetic field. The corresponding frequency shift is independent of h , as demonstrated by Eq. (9). On the other hand, the translation around the circumference of the cavity, i.e., the change in ϕ significantly changes the frequency shift ν^\pm . Therefore, deuterons in molecules found at different angular coordinates resonate at different frequencies $\nu^\pm = f(\nu_q, Q, \eta; \Psi_0, \Theta_0, \Phi_0; \phi, \theta)$. The five unknowns—the order parameter components (Q, η) as well as the orientation (Ψ_0, Θ_0, Φ_0) of its eigensystem with the respect to the local frame can depend on the molecular position (h, ϕ), or alternatively, vary stochastically along the surface. In such a most general case this makes it unfeasible, without further simplifications of f , to determine the above unknowns and their possible distributions or (h, ϕ)—dependencies from the distribution of the deuteron NMR absorption frequencies.

B. Symmetry considerations in a cylindrical geometry

On smooth, flat surfaces, the long axis of a nonadsorbed (not frozen at the surface) 5CB molecule is expected to exhibit uniaxial dynamic reorientations around the surface nor-

mal, equivalently, homeotropic alignment. This includes the case where a molecule lies flat on the surface whereas its long molecular axis reorients in the surface plane ($Q = -1/2$) [24]. However, the symmetry of the ordering tensor must reflect the symmetry of local environment, which is not cylindrical due to a slight surface curvature, i.e., one must permit confinement-induced biaxial ordering ($\eta \neq 0$). This can be taken into account by considering the eigensystem of the order parameter must coincide with the one dictated by the pore geometry, i.e., the local coordinate system \mathbf{xyz} matches the eigensystem \mathbf{XYZ} . Then $R_{xyz \rightarrow XYZ}(\Psi_0, \Theta_0, \Phi_0)$ is an identity matrix and consequently

$$\nu^\pm = \pm \frac{1}{8} \nu_q Q [3 \sin^2 \theta \cos^2 \phi - 1 + \eta (\sin^2 \theta \sin^2 \phi - \cos^2 \theta)]. \quad (11)$$

Let us now further assume homogeneous molecular order, namely, that Q and η do not depend on the position of the molecule on the surface. The deuteron line shape $I(\nu)$ is given by

$$I(\nu) = \frac{I(\nu^+) + I(\nu^-)}{2}, \quad (12a)$$

$$I(\nu^\pm) = \frac{1}{N} \frac{dN}{d\phi} \left| \frac{d\nu^\pm}{d\phi} \right|^{-1}. \quad (12b)$$

N is the number of resonating nuclei. In a molecular film of homogeneous surface coverage $A \neq A(h, \phi)$ the angular distribution is also constant, $dN/d\phi = N/2\pi$. We then find

$$\begin{aligned}I(\nu^\pm) &= \frac{2}{\pi \nu_q Q} \left[\left((\eta + 3) \sin^2 \theta - 1 - \eta \mp \frac{8\nu}{\nu_q Q} \right) \right. \\ &\times \left. \left(\pm \frac{8\nu}{\nu_q Q} + 1 + \eta - 2\eta \sin^2 \theta \right) \right]^{-1/2}.\end{aligned}\quad (13)$$

Angular dependencies of the above line shapes are shown in Fig. 3(a) for a few representative values of η . The above line-shape angular dependence is similar to the one found for planar radial and planar polar director configurations; the latter was shown to exist in the long chain aliphatic acid treated Anopore, filled completely with 5CB [14]. At a general orientation θ of the sample, two pairs of spectral singularities are visible [Fig. 3(b)] at the two respective frequency pairs,

$$\nu_I^\pm(Q, \eta; \theta) = \pm \frac{\nu_q Q}{8} [(\eta + 3) \sin^2 \theta - \eta - 1] \quad (14a)$$

and

$$\nu_{II}^\pm(Q, \eta; \theta) = \pm \frac{\nu_q Q}{8} [2\eta \sin^2 \theta - \eta - 1]. \quad (14b)$$

The two singularity doublets ν_I^\pm and ν_{II}^\pm correspond to angular locations $\phi_I = 0, \pi$ and $\phi_{II} = \pi/2, 3\pi/2$, respectively.

At $\theta = 0$, ν^\pm does not depend on ϕ . Then, the spectrum consists of a doublet of frequency separation

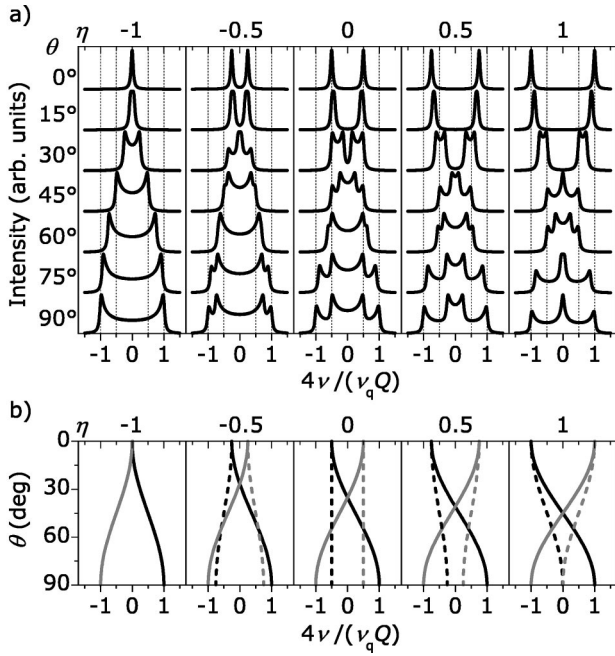


FIG. 3. (a) Angular dependence of theoretical DNMR spectra for several values of the asymmetry parameter η . To account for homogeneous line shape broadening, the spectra are convoluted with a $\Delta\nu_{\text{hom}} = 0.08 \nu_q Q/4$ Lorentzian; (b) angular dependencies of spectral singularities ν_I (solid lines) and ν_{II} (dashed lines). The black lines correspond to the “+” satellite transition and the gray lines to the “-” satellite transition.

$$\Delta\nu_S = -\frac{1}{4}\nu_q Q(1+\eta). \quad (15)$$

Here the index S is used for “surface” to emphasize the 2D nature of the surface deposition. The surface order parameter and its biaxiality can be determined from the singularity splittings $\Delta\nu_I = \nu_I^+ - \nu_I^-$ and $\Delta\nu_{II} = \nu_{II}^+ - \nu_{II}^-$, measured at the $\theta = \pi/2$ orientation,

$$Q = \frac{2\Delta\nu_I(\pi/2)}{\nu_q}, \quad (16a)$$

$$\eta = 1 + \frac{2\Delta\nu_{II}(\pi/2)}{\Delta\nu_I(\pi/2)}. \quad (16b)$$

This behavior is significantly different from that in full, untreated Anopore [21], where only a single spectral doublet with a bulklike frequency splitting

$$\Delta\nu_B = \frac{1}{2}\nu_q Q_B P_2(\cos\theta) \quad (17)$$

is detected at any sample orientation θ . Here Q_B denotes the bulk nematic order parameter. Equations (15) and (17) can be combined to yield the relation

$$\frac{\Delta\nu_S}{\Delta\nu_B}(\theta=0) = \frac{2Q(1+\eta)}{Q_B}, \quad (18)$$

which can be used to estimate the orientational order Q of the surface deposition, provided that Q_B is determined from an independent measurement of the bulk doublet angular dependence.

V. MOLECULAR SELF-DIFFUSION

In the above discussion, the molecular translational diffusion on the alumina surface was not considered. If, however, during the DNMR signal detection period a molecule travels a considerable distance leading to changes in its resonance frequency $\nu(\theta, \phi)$, motional averaging of the DNMR spectra will take place. Specifically, substantial averaging occurs if on the DNMR experimental time scale τ_{DNMR} a diffusing molecule scans all possible frequencies. In order to achieve that, it must travel an angular distance of at least $\Delta\phi \approx 1$ around the circumference of the cavity. The width of the respective frequency interval is

$$\Delta\nu_{\text{rig. latt.}} = |\nu_I^+ - \nu_{II}^+| = |\nu_I^- - \nu_{II}^-| = \frac{\nu_q |Q(3-\eta)|}{8} \sin^2\theta, \quad (19)$$

the characteristic “rigid lattice” DNMR line width, obtained in the absence of diffusion. This quantity determines the time scale τ_{DNMR} via $\tau_{\text{DNMR}} \approx \Delta\nu_{\text{rig. latt.}}^{-1}$. For a diffusion process with a Gaussian-type propagator, $\Delta\phi \approx \sqrt{\langle \Delta\phi^2 \rangle}$ and τ_{DNMR} can be related via $r_0^2 \langle \Delta\phi^2 \rangle = 2D_S \tau_{\text{DNMR}}$. Combining the above relations we obtain the characteristic surface diffusion constant

$$D_S^{\text{NMR}} \approx D_{S0}^{\text{NMR}} |Q(1-\eta/3)| \sin^2\theta, \quad (20a)$$

$$D_{S0}^{\text{NMR}} = 3r_0^2 \nu_q / 16. \quad (20b)$$

In the slow diffusion regime, $D_S \ll D_S^{\text{NMR}}$, there are no motional averaging effects and DNMR probes the “rigid lattice,” i.e., the zero diffusion limit line shape as given by Eq. (13). For faster diffusion, $D_S \approx D_S^{\text{NMR}}$, motional narrowing sets in. With increasing D_S , this regime is reached sooner in a system with smaller pore radii and higher orientational order. Diffusion effects are also more pronounced at smaller sample tilts. In the fast diffusion limit, $D_S \gg D_S^{\text{NMR}}$, the DNMR spectrum is averaged out completely. Its angular dependence can be calculated by noting that in this regime, every molecule travels on the DNMR time scale several times around the cavity circumference, thus, the diffusion-averaged orientational order parameter tensor of any molecule possesses uniaxial symmetry with the symmetry axis parallel to the cavity axis. The effective molecular order is similar to that in full untreated Anopore [21] where at any orientation a sharp doublet with a splitting proportional to $P_2(\cos\theta)$ is found. At $\theta=0$, the resonance frequency does not depend on the angular coordinate ϕ [see Eq. (11)]; DNMR is unable to distinguish if the molecules diffuse or not. The zero diffusion limit and fast diffusion limit spectra are identical at $\theta=0$ and consist of the doublet with frequency splitting given by Eq. (15). At a general orientation, the doublet splitting in the $D_S \gg D_S^{\text{NMR}}$ limit is then

$$\Delta \nu_{S,D} = -\frac{1}{4} \nu_q Q (1 + \eta) P_2(\cos \theta), \quad (21)$$

with the index D representing the diffusion-induced change in the DNMR spectrum.

In our system, $D_{50}^{\text{NMR}} = 3.4 \times 10^{-10} \text{ m}^2 \text{ s}^{-1}$; at any sample orientation, $|Q(1 - \eta/3)| \sin^2 \theta \leq 1$ is also satisfied, so that $D_S^{\text{NMR}} \leq 3.4 \times 10^{-10} \text{ m}^2 \text{ s}^{-1}$. To estimate the effect of diffusion, we shall assume that the surface diffusion constant D_S is not too different from that of bulk 5CB: $D_S \approx D_{5\text{CB}}$, with $D_{5\text{CB}} \approx 5.5 \times 10^{-11} \text{ m}^2 \text{ s}^{-1}$ in the isotropic phase at $T = 310 \text{ K}$ and $\approx 7.5 \times 10^{-11} \text{ m}^2 \text{ s}^{-1}$ in the nematic phase at $T = 300 \text{ K}$ [33]. At sufficiently small values of Q , $D_S \geq D_S^{\text{NMR}}$ is satisfied, i.e., diffusion-induced motional averaging sets in even at $\theta = \pi/2$ where it is least effective. In general we thus deal with different NMR line-shape averaging regimes: fast motion limit at small sample tilts, intermediate case at intermediate tilts and slow motion limit for $\theta \rightarrow \pi/2$.

In the intermediate regime $D_S \approx D_S^{\text{NMR}}$, the DNMR line shape is only partially averaged out and neither Eq. (13) nor Eq. (21) describe the spectrum adequately. Under such conditions, the line shape has to be calculated using a general approach, namely, by Fourier transforming the diffusion-modulated deuteron nuclear magnetization decay in time. This decay obeys the diffusion equation [34]

$$\begin{aligned} \frac{\partial M(\phi, t)}{\partial t} &= i 2\pi \nu^\pm(\phi) M(\phi, t) - \frac{M(\phi, t)}{T_2} \\ &+ \frac{D_S}{r_0^2} \frac{\partial^2 M(\phi, t)}{\partial \phi^2}, \end{aligned} \quad (22)$$

with $\nu^\pm(\phi)$ as defined by Eq. (11). Although a diffusing molecule moves in three dimensions, the problem is first reduced to two dimensions by unfolding the cylindrical surface of the cavity into a plane with coordinate space $(r_0\phi, h)$, and then to one dimension by noting that $\nu^\pm(\phi)$ is independent of h . T_2 is the spin-spin relaxation time that describes the effects of all magnetization-dephasing mechanisms excluding diffusion. It is taken as ϕ independent for simplicity reasons. The detectable NMR decay $M(t)$ is a superposition of signals originating from all angular positions, $\int_0^{2\pi} M(\phi, t) dt$. Solving Eq. (22) for $M(t)$ then makes it possible to calculate the DNMR line shape from the Fourier transformation $I^\pm(\nu) \propto \int_0^\infty M(t) \exp(-i 2\pi \nu^\pm t) dt$. A solution for Eq. (22) can be found in an elegant way by rewriting the derivatives in terms of differences,

$$\begin{aligned} \frac{dM_k(t)}{dt} &= i 2\pi \nu_k M_k(t) - \frac{M_k(t)}{T_2} + \frac{D_S}{r_0^2 \Delta \phi^2} [M_{k+1}(t) \\ &- 2M_k(t) + M_{k-1}(t)]. \end{aligned} \quad (23)$$

This is done by partitioning the $\phi \in [0, 2\pi]$ continuous coordinate space into a N -dimensional space of equally spaced coordinates $\phi_k = k\Delta\phi$ where $k = 1, 2, \dots, N$ and $\Delta\phi = 2\pi/N$, as well as replacing $\nu^\pm(\phi) \rightarrow \nu_k^\pm$ and $M(\phi, t)$

$\rightarrow M(\phi_k, t) = M_k(t)$. One can then introduce a N -component magnetization vector $\mathbf{M}(t) = \{M_k(t)\}$, a $N \times N$ component diagonal matrix of frequencies $\underline{\nu}^\pm = \{\nu_k^\pm \delta_{kl}\}$, and a $N \times N$ component ‘‘exchange’’ matrix, where only its nonzero elements are shown below:

$$K = \begin{bmatrix} -2 & 1 & & & & & 1 \\ & 1 & -2 & 1 & & & \\ & & 1 & -2 & 1 & & \\ & & & \ddots & & & \\ & & & & 1 & -2 & 1 \\ & & & & & 1 & -2 & 1 \\ 1 & & & & & & & 1 & -2 \end{bmatrix} \frac{D_S}{r_0^2 \Delta \phi^2}. \quad (24)$$

Then, Eq. (23) can be recast in the form of N linear population equations,

$$\frac{d\mathbf{M}(t)}{dt} = [i 2\pi \underline{\nu}^\pm - T_2^{-1} \underline{1} + K] \mathbf{M}(t) \quad (25)$$

with solution

$$\mathbf{M}(t) = \exp[(i 2\pi \underline{\nu}^\pm - T_2^{-1} \underline{1} + K)t] \mathbf{M}(0). \quad (26)$$

Here $\underline{1}$ is a N -dimensional identity matrix. At any given time all angular coordinates are equally probable, hence $\mathbf{M}(0) \propto \mathbf{1} = [1, 1, \dots, 1]$. The frequency spectrum is obtained by Fourier transforming $\mathbf{M}(t)$,

$$\mathbf{I}^\pm(\nu) \propto \int_0^\infty \exp[-i 2\pi \nu \underline{1} \cdot t] \mathbf{M}(t) dt = \kappa^{-1}(\nu) \mathbf{1}, \quad (27a)$$

$$\kappa(\nu) = i 2\pi (\underline{\nu}^\pm - \nu \underline{1}) - T_2^{-1} \underline{1} + K. \quad (27b)$$

An individual component I_k^\pm of the above intensity vector corresponds to the amount of signal originating from the angular interval $\phi \in [\phi_k - \Delta\phi/2, \phi_k + \Delta\phi/2]$. The experimentally detected line shape is the real part of the sum over all components,

$$I^\pm(\nu) \propto \text{Re}\{\mathbf{1}^T \kappa^{-1}(\nu) \mathbf{1}\}. \quad (28)$$

We have thus converted the complex problem of solving the diffusion Eq. (22) to a simple calculation of the inverse of the matrix $\kappa(\nu)$. The resulting spectrum reproduces the true diffusion case only in the $N \rightarrow \infty$ limit. However, the actual N required to obtain a satisfactory resemblance is set by the homogeneous line width $\Delta\nu_{\text{hom}}$, i.e., the spectral width of a signal corresponding to nondiffusing molecules at an angular coordinate ϕ , related to T_2 via $\Delta\nu_{\text{hom}} = (\pi T_2)^{-1}$. N must be chosen large enough that $\Delta\nu_{\text{hom}}$ exceeds the inhomogeneous frequency resolution $\Delta\nu_{\text{rig. latt}}/N$. Using Eq. (19), this results in the criterion

$$N \geq \frac{\pi T_2 \nu_q Q (3 - \eta)}{8} \sin^2 \theta. \quad (29)$$

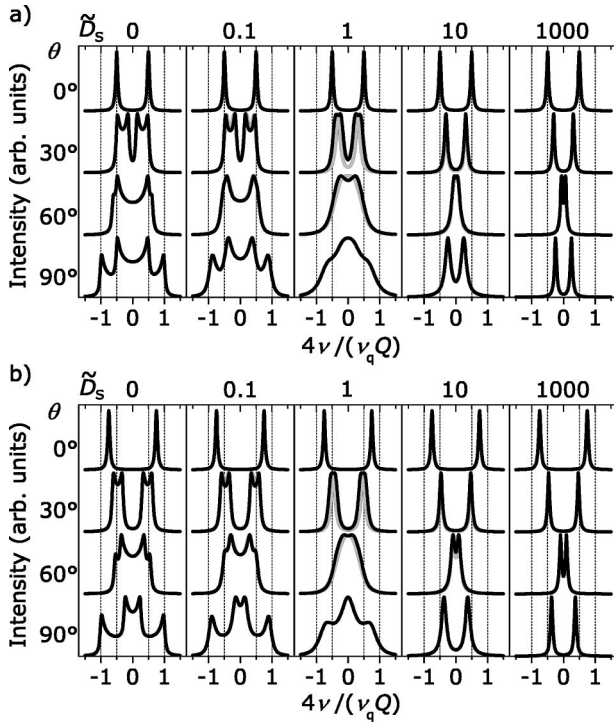


FIG. 4. Angular dependence of theoretical DNMR spectra in different, \tilde{D}_S -characterized diffusion regimes for (a) $\eta=0$ and (b) $\eta=0.5$ ($\tilde{\Delta\nu}_{\text{hom}}=0.08$). Black lines were calculated with \tilde{D}_S values as specified, whereas the gray lines were obtained with $\tilde{D}_S \sin^2\theta$. They overlap almost perfectly, except for the discrepancy in the transition region $\tilde{D}_S \approx 1$, particularly pronounced at $\theta=30^\circ$. This demonstrates that stronger averaging takes place at smaller θ (the discrepancy is not visible at very small θ for there the line shapes are diffusion invariant).

Let us now consider the worst case scenario: $Q=1$, $\eta=0$, $\theta=\pi/2$, and $T_2 \rightarrow T_1$ (T_2 cannot exceed T_1). Using the bulk 5CB values $\nu_q \approx 180$ kHz and $T_1 \approx 15$ ms [33] one obtains $N \geq 3000$. For smaller order parameter values and smaller sample tilts, this reduces to $N \approx 100$.

It is straightforward to show that DNMR spectrum given by Eq. (28) can be expressed in a dimensionless form $I^\pm(\tilde{\nu}; \eta, \theta, \tilde{\Delta\nu}_{\text{hom}}, \tilde{D}_S)$ in terms of the dimensionless frequency $\tilde{\nu}=4\nu/(\nu_q Q)$ and the dimensionless parameters $\tilde{\Delta\nu}_{\text{hom}}=4\Delta\nu_{\text{hom}}/(\nu_q Q)$ and $\tilde{D}_S=D_S/D_S^{\text{NMR}}$. Diffusion-induced averaging effects are illustrated in Fig. 4 for several values of the dimensionless diffusion rate \tilde{D}_S . The calculation of angular patterns with constant \tilde{D}_S , despite providing the most elegant approach in view of the \tilde{D}_S dimensionlessness, implies a θ -dependent diffusion rate D_S [see Eq. (20)], an experimentally unrealistic scenario. This is why a second set of theoretical spectra is also shown in Fig. 4, calculated with $\tilde{D}_S \sin^2\theta$, i.e., with θ -independent diffusion rate D_S . In general, the rigid-lattice ($\tilde{D}_S \leq 1$) spectra gradually smear out on approaching the $\tilde{D}_S \approx 1$ regime, and subsequently develop into a sharp resonance doublet in the $\tilde{D}_S \gg 1$ limit. In the case of a slow diffusion ($\tilde{D}_S < 1$), the averaging results in

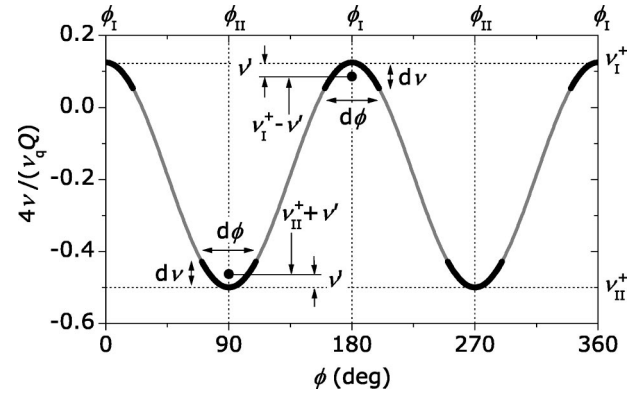


FIG. 5. Schematic representation of effective spectral singularity shift ν' due to molecular diffusion for a system with $\eta=0.5$ at an orientation $\theta=\pi/4$. The fluctuation of the phase angle $d\phi \approx \sqrt{2D_S dt}$ about $\phi_I=0, \pi$ and $\phi_{II}=\pi/2, 3\pi/2$, respectively, during the signal detection period dt corresponds to frequency fluctuation $d\nu$ around ν_I^+ and ν_{II}^+ , respectively. At slow diffusion, $\tilde{D}_S \ll 1$, this is detected as a single averaged frequency response with $\nu_I^+ - \nu'$ in the ϕ_I singularities and $\nu_{II}^+ + \nu'$ in the ϕ_{II} singularities. This interpretation is valid for any θ and η as $\nu(\phi)$ always retains its $\cos^2\phi$ dependence [Eq. (11) can be recast into $\nu(\phi) \propto a(\theta, \eta) + b(\theta, \eta)\cos^2\phi$]. Only the “+” satellite line of the doublet is shown.

a shift of the singularity positions. This can be explained by examining the ϕ dependence of the rigid-lattice frequency shift in Eq. (11), schematically presented in Fig. 5. For symmetry reasons, the effective frequency shifts of the singularities have the same amplitude $\nu'(Q, \eta, D_S; \theta)$, but opposite directions. We can, therefore, write

$$\nu_I^\pm(Q, \eta, D_S < D_S^{\text{NMR}}; \theta) \approx \nu_I^\pm(Q, \eta; \theta) \mp \nu'(Q, \eta, D_S; \theta) \quad (30a)$$

and

$$\nu_{II}^\pm(Q, \eta, D_S < D_S^{\text{NMR}}; \theta) \approx \nu_{II}^\pm(Q, \eta; \theta) \pm \nu'(Q, \eta, D_S; \theta). \quad (30b)$$

At this point it is worth pointing out the close analogy that exists between a cholesteric LC DNMR spectra, investigated by Chidichimo and coauthors [35], and the DNMR line shapes found here. From the DNMR perspective, the precession of the molecular director on moving along the symmetry axis of a cholesteric LC structure is analogous to the reorientation of the molecular director as the molecule moves around the circumference of a cylindrical cavity. In Ref. [35], an analytical approximation for the diffusion-induced shift ν' was calculated for a specific $\theta=\pi/2$ orientation, with θ measuring the angle between the cholesteric axis and the external magnetic field. The cholesteric pitch p_0 can be replaced with the circumference $2\pi r_0$ so that $\nu'(Q, \eta, D_S; \pi/2)$, adapted to our system, becomes

$$\nu'(Q, \eta, D_S; \pi/2) = \frac{\nu_q Q}{16} (3 - \eta) U(Q, D_S), \quad (31a)$$

where

$$U(Q, D_S) = 1 - \frac{\nu_q Q r_0^2}{24 D_S} \left[1 - \exp\left(-\frac{24 D_S}{\nu_q Q r_0^2}\right) \right]. \quad (31b)$$

As discussed in Ref. [35], numerical factors in Eqs. (31) may be incorrect due to some rather crude approximations made in their derivation. The most important property of Eqs. (30) is the invariance of the sum of the singularity positions to diffusion,

$$\begin{aligned} \nu_I^\pm(Q, \eta, D_S < D_S^{\text{NMR}}; \theta) + \nu_{\text{II}}^\pm(Q, \eta, D_S < D_S^{\text{NMR}}; \theta) \\ = \frac{\nu_q Q (\eta + 1)}{8} (3 \sin^2 \theta - 2), \end{aligned} \quad (32)$$

which allows to measure the value of the product $Q(\eta + 1)$ even in the presence of diffusion. Unfortunately, Q and η cannot be determined separately, since, unlike the cholesteric LC's case [36], no equivalent system can be used for an independent measurement of Q . Hence, the only reliable approach to determine Q , η , and D_S is by fitting the angular dependence of the spectra.

Without diffusion, singularity splittings can be used to determine Q and η using Eqs. (16). In the presence of diffusion we have

$$\Delta \nu_I(\theta = 0) = -\frac{\nu_q Q}{4} (\eta + 1), \quad (33a)$$

$$\Delta \nu_I(\theta = \pi/2) = \frac{\nu_q Q}{2} - 2\nu'(Q, \eta, D_S; \pi/2), \quad (33b)$$

and

$$\Delta \nu_{\text{II}}(\theta = \pi/2) = \frac{\nu_q Q}{4} (\eta - 1) + 2\nu'(Q, \eta, D_S; \pi/2). \quad (33c)$$

These relations are dependent on each other through

$$\Delta \nu_I(0) + \Delta \nu_I(\pi/2) + \Delta \nu_{\text{II}}(\pi/2) = 0, \quad (34)$$

due to the tracelessness of the orientational order parameter tensor. As a consequence, Q , η , and D_S cannot be determined simultaneously from Eqs. (33). However, in the uniaxial case ($\eta = 0$), they yield two measurable parameters

$$Q_D = -\frac{4\Delta \nu_I(0)}{\nu_q}, \quad (35a)$$

$$\eta_D^{\text{eff}} = 1 + \frac{2\Delta \nu_{\text{II}}(\pi/2)}{\Delta \nu_I(\pi/2)}. \quad (35b)$$

The index D standing for ‘‘diffusion’’ is used with Q and η^{eff} to emphasize that they are determined assuming $D_S \neq 0$ and $\eta = 0$. D_S can in turn be determined from the known values of Q_D and η_D^{eff} by solving the transcendental equation

$$\eta_D^{\text{eff}} = 1 - \frac{4 - 6U(Q, D_S)}{4 - 3U(Q, D_S)}, \quad (36)$$

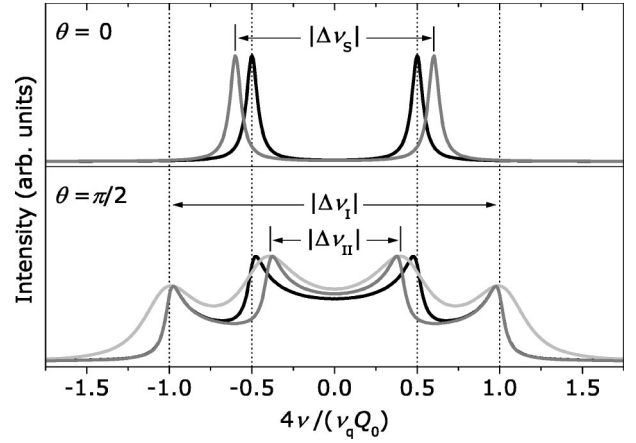


FIG. 6. Theoretical DNMR spectra of surface-deposited 5CB molecules in the case of inherent biaxial ordering, calculated with parameters $Q = Q_0$, $\eta = \eta_0 = 0.2$, $D_S = 0$ (dark gray lines) and in the case of slow diffusion, calculated with parameters $Q_D = Q_0(1 + \eta_0)$, $\eta = 0$, $D_S(\eta_D^{\text{eff}} = \eta_0) \neq 0$ (light gray lines). A minor mismatch in the position of the maxima of the two models is attributed to an approximate-only value of the numerical factor of Eq. (37) [see Eqs. (31) and the associated text]. The $\eta = 0$, $D_S = 0$ case is also shown for comparison (black lines).

which, for $D_S < D_S^{\text{NMR}}$, can be linearized to yield

$$D_S \approx \frac{16}{27} Q D_{S0}^{\text{NMR}} \eta_D^{\text{eff}}. \quad (37)$$

This demonstrates that slow diffusion yields an effective biaxiality η_D^{eff} . It is thus difficult to resolve between inherent biaxiality and diffusion effects. This is well manifested, for small η and D_S , in the matching maxima positions of the $D_S = 0$, $\eta \neq 0$ and the $D_S \neq 0$, $\eta = 0$ spectra of Fig. 6. Nevertheless, the nuclear magnetization decay due to diffusion is of a dynamic nature and results in a homogeneous broadening of the DNMR spectrum. The solution to Eq. (23) for a given k is not an exponential function—in other words, the contribution of diffusion to the homogeneous spectral component from the molecules found on the average at an angular coordinate $\phi(k)$ is in general not a Lorentzian. In the slow diffusion limit, $D_S \ll D_S^{\text{NMR}}$, one can disregard the mixing ($k \mp 1$) terms, so that the diffusion effectively results in an increased spin-spin relaxation rate $1/T_2^{\text{eff}} = 1/T_2 + 1/T_2^D$ with $T_2^D \propto D_S^{-1}$. As noted earlier, at $\theta = 0$, diffusion is ineffective and $T_2^{\text{eff}} = T_2$. At $\theta > 0$, on the other hand, $T_2^{\text{eff}} < T_2$, and the spectral singularities are broadened with respect to rather sharp inherent biaxiality case singularities (see the $\theta = \pi/2$ spectra of Fig. 6). The orientation dependent T_2^{eff} is therefore an indicator of the diffusion averaging of the DNMR line shapes.

VI. EXPERIMENTAL RESULTS

A. Experimental details

DNMR spectra of 5CB- ad_2 films in Anopore were obtained by $90_x^0 - 90_y^0$ ‘‘solid echo’’ pulse sequence in \mathbf{B}_0

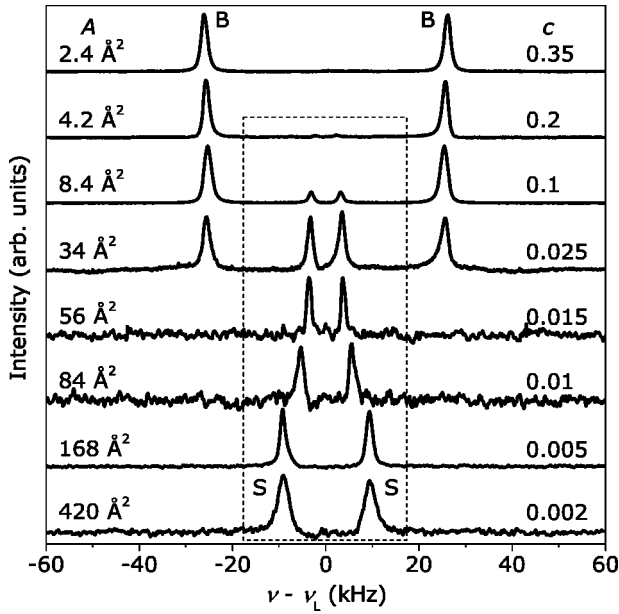


FIG. 7. Batch II DNMR spectra, recorded at $\theta=0$ and T_{room} . B denotes the bulk component. Molecular deposition at the surface, denoted by S , exhibits a reduced doublet splitting (dotted frame).

= 4.73 T and $\mathbf{B}_0=9$ T superconducting magnets at the ^2H Larmor frequencies $\nu_L=30.9$ MHz and $\nu_L=58.3$ MHz, respectively. Results were perfectly reproducible in both magnetic field strengths at any arbitrary orientation of the samples, demonstrating that no magnetic field induced orientational effects are present.

Samples of various surface coverages $A(c)$ [see Eq. (2)] were prepared from two different Anopore batches, I and II, with the same nominal pore diameter $d_0=2r_0=200$ nm. Preliminary results for films formed in batch I were reported in Ref. [8]. A more extensive investigation was then performed with batch II; we present here the combined results. Except for some minor quantitative differences, which will be discussed below, qualitatively the results do not depend on the Anopore batch.

B. Surface coverage dependence of the resonance spectra

DNMR line shapes at $\theta=0$ orientation for a few representative samples of batch II, measured at $T_{\text{room}}=298$ K, are shown in Fig. 7. The spectra for samples with $A(c \geq 0.35) \leq 2.4 \text{ \AA}^2 = A_1(c_1)$ all display a characteristic bulk nematic doublet (denoted by B). Its frequency splitting $\Delta\nu_B$ is proportional to the nematic order parameter Q_B , in accordance with Eq. (17). Decreasing the filling factor c , or equivalently, increasing the area per molecule A , a second frequency doublet appears which coexists with the bulk one. Let us denote this new doublet by S as we speculate that it originates from the surface deposition of liquid crystal molecules. The relative intensity of the S doublet, measured against the bulk doublet intensity, increases with decreasing c . The bulk part completely vanishes above $A(c \leq 0.02) \geq 42 \text{ \AA}^2 = A_2(c_2)$. Coincidentally, this value also characterizes the 2D-liquid phase of 5CB at an air-water interface [11]. A remarkable feature is the lack of gradual development of bulk order,

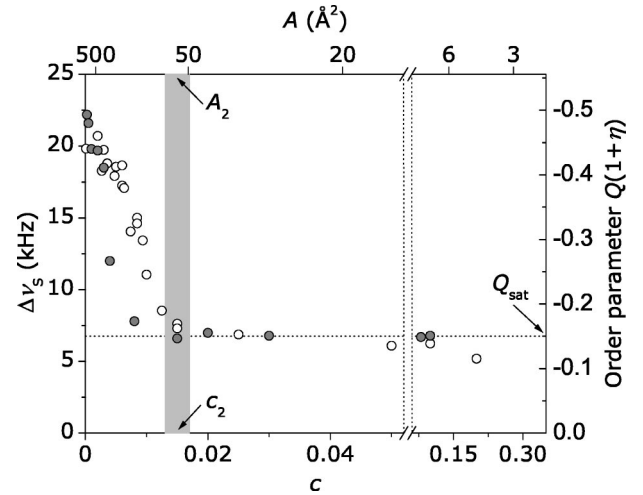


FIG. 8. 5CB surface deposition DNMR absorption doublet frequency splitting as a function of surface coverage for batches I (solid circles) and II (open circles). The span of the $Q(1+\eta)$ order parameter product's vertical scale is set by $\nu_q=180$ kHz [Eq. (15)].

described quantitatively by Q_B , into the surface order (characterized by Q), in the $A_1 < A < A_2$ ($c_2 < c < c_1$) interval. It would thus appear that the only possible molecular states are the “bulk” one and the “surface” one. The previous observation contains all the characteristics of a dewetting scenario [7] where molecular depositions with $A > A_1$ tend to dewet into the bulk, leaving the dewetted regions covered with a thin molecular film, deposited at the air/solid interface. The properties of such a film are governed by the interface and the resulting molecular orientational order at the surface agrees with the discussion in Sec. IV B. Explicitly, the surface layer doublet splitting $\Delta\nu_S$ is proportional to the surface orientational order Q . Experimentally determined values of $\Delta\nu_S \propto Q(1+\eta)$ are shown in Fig. 8. In the region where the surface component coexists with the bulk, $\Delta\nu_S \approx 5-7$ kHz and hence $Q(1+\eta) \approx -0.15$ is practically independent of c . This is to be expected since on dewetting, the thermodynamically stable surface layers remaining on the exposed areas, most likely, have similar molecular configurations and a well defined, homogeneous effective thickness and consequently, a homogeneous Q . Let us call such a film coexisting with bulk, a “saturated film,” and denote the respective order parameter with $Q_{\text{sat}}=Q(c > c_2)$. The excess material is all collected in the bulklike phase. Below c_2 , however, there is no excess LC material left to dewet. Then, since the surface density of the molecules is too low for the formation of the saturated film, the orientational order must depend on c for $c < c_{\text{II}}$. The strong, quasilinear increase of $Q \propto \Delta\nu_S$ below c_2 , seen in Fig. 8, indeed reflects this situation. In the limit of infinite area per molecule ($c \rightarrow 0$, $A \rightarrow \infty$), $\Delta\nu_S \approx 22.5$ kHz, corresponding to $Q \approx -1/2$. The above results agree with a scenario where on decreasing surface coverage from the saturated film to infinite dilution ($A \rightarrow \infty$), the orientational order parameter changes from $-1/2 < Q_{\text{sat}} < -1$ to $Q = -1/2$ (Fig. 9). It should be stressed that the sign of Q cannot be determined through deuteron quadrupole-perturbed NMR experiment due to the \pm sign in Eq. (11). Thus, one is limited

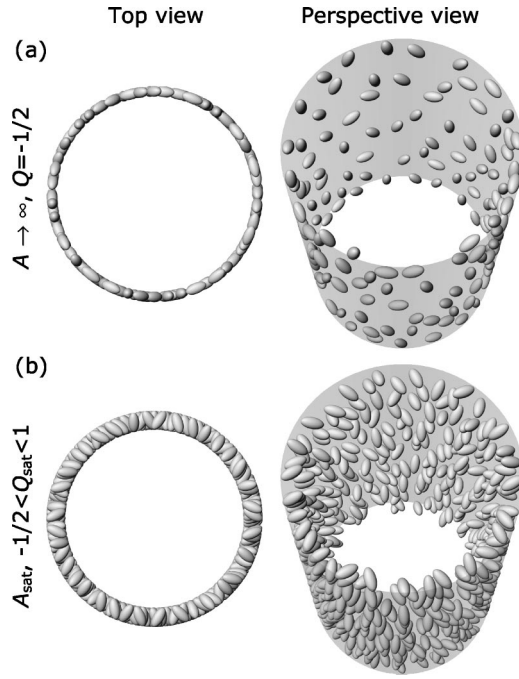


FIG. 9. A schematic picture of 5CB molecular arrangement at the Anopore inner surface for two different surface coverages: a highly diluted deposition (a) and a saturated molecular deposition (b). The molecular size is exaggerated with respect to the pore radius.

to conclude that $|Q| \rightarrow 1/2$ in the $A \rightarrow \infty$ limit. As already stated, $Q \approx -1/2$ whenever the molecular long axes lie flat on the surface and reorient quickly on the NMR time scale in a uniaxial fashion with the axis of symmetry perpendicular to the surface. If the saturated value of Q_{sat} were positive, $Q_{\text{sat}} \approx 0.15$, then on approaching the $A \rightarrow \infty$ limit with $Q = -1/2$, $Q(A(c))$ would have to cross zero in order to become negative; since this was not observed (Fig. 8), we conclude that $Q_{\text{sat}} = -0.15$ and $Q < 0$ for any $A(c)$. In terms of the language introduced for full Anopore, the molecular configuration of the surface layer is planar radial with a negative orientational order parameter. The planar polar configuration can be excluded, for in a 2D system the contribution of line singularities with zero Q is not negligible, in contrast to 3D systems (full Anopore). If singularities were present in surface depositions, they would contribute to the deuteron NMR spectra as quasi-isotropic absorption peaks with zero frequency shift; as evident from Fig. 7, such is not the case.

C. Angular dependence of the resonance spectra

Deuteron NMR line-shape θ dependencies were measured with the $c_{\text{II}}=0.1$ sample at $T=310 \text{ K} > T_{\text{NI}}$ and at $T_{\text{room}} < T_{\text{NI}}$. Measurements were also performed with the $c_{\text{II}}=0.005$ and $c_{\text{I}}=0.004$ samples at T_{room} .

The small splitting of the DNMR spectra in the isotropic phase of the $c_{\text{II}}=0.1$ sample (Fig. 10) exhibits a typical $P_2(\cos \theta)$ angular dependence, and reveals the presence of the bulk phase orientational wetting at the cavity walls [14]. The S spectral component, related to the dewetted surface layer, is traceable at $T > T_{\text{NI}}$ only at small sample tilts be-

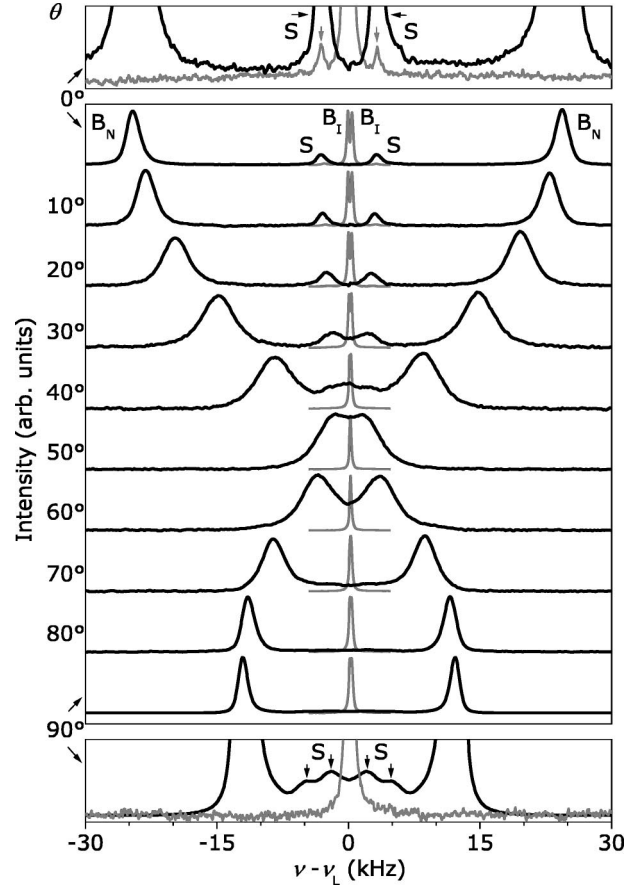


FIG. 10. Experimental θ -dependence spectral patterns of the $c_{\text{II}}=0.1$ system in which bulk (B) component and surface (S) components coexist. Gray solid lines were measured at $T=310 \text{ K} > T_{\text{NI}}$ and black solid lines at $T_{\text{room}} < T_{\text{NI}}$. In the isotropic phase, a small splitting of the bulk isotropic absorption peak (B_I) is visible. Below T_{NI} , the bulk component is seen as a single doublet (B_N) at any orientation. The surface layer deposition component (S) transforms from a doublet at $\theta=0$ into a four maxima structure, reminiscent of cylindrical symmetry, at $\theta=\pi/2$.

cause of a rather weak signal-to-noise ratio in this particular scan. At $T < T_{\text{NI}}$ where the bulk part is in the nematic phase, this component is clearly visible. Here, the magnitude of the bulk nematic splitting is $\Delta \nu_B \approx 49 \text{ kHz}$ while the surface component exhibits a $\Delta \nu_S \approx 6.4 \text{ kHz}$ splitting. The angular dependence of the spectra of Fig. 10 clearly demonstrates that the difference in the frequency splitting between bulk and surface phases is not only a consequence of a decreased orientational order Q in the surface phase as compared to bulk, but also due to a different configurational symmetry: the bulk part angular dependence is clearly of the $P_2(\cos \theta)$ type and corresponds to a parallel axial arrangement [14], whereas the surface deposition part conforms to the angular frequency pattern described by Eqs. (13) or (28) and thus agrees with a planar radial arrangement, as proposed for the surface-deposited molecules in Sec. VI B.

Because of the superimposed bulk component, it is tedious to determine the values of Q , η , and D_S in the dewetted molecular deposition from the $c_{\text{II}}=0.1$ angular dependencies; an estimation was nevertheless made using Eqs.

TABLE I. Best fit parameters Q and η for the pure biaxiality ($\eta \neq 0$, $D_S = 0$) model and best fit parameters Q_D , η_D^{eff} and D_S for the pure diffusion ($\eta \neq 0$, $D_S \neq 0$) model for three different surface coverages (the respective columns are sorted in the order of increasing $|\Delta \nu_s(\theta=0)|$) at $T=300$ K. The better fitting model's parameters are shown in boldface.

c_{batch}	0.1 _{II}	0.004 _I	0.005 _{II}
$ \Delta \nu_s(\theta=0) $ (kHz)	$6.2 \times (1 \pm 0.05)$	$12.5 \times (1 \pm 0.02)$	$16.6 \times (1 \pm 0.02)$
$\Delta \nu_0$ (kHz)	$2.3 \times (1 \pm 0.02)$	$0.9 \times (1 \pm 0.02)$	$2.2 \times (1 \pm 0.02)$
$ Q $	$0.11 \times (1 \pm 0.1)$	$0.24 \times (1 \pm 0.07)$	$0.37 \times (1 \pm 0.07)$
η	$0.24 \times (1 \pm 0.3)$	$0.13 \times (1 \pm 0.3)$	0 ± 0.03
$ Q_D $	$0.14 \times (1 \pm 0.1)$	$0.27 \times (1 \pm 0.08)$	$0.37 \times (1 \pm 0.08)$
η_D^{eff}	$0.24 \times (1 \pm 0.3)$	$0.13 \times (1 \pm 0.3)$	0 ± 0.03
D_S ($10^{-12} \text{ m}^2 \text{ s}^{-1}$)	$6.6 \times (1 \pm 0.5)$	$7.0 \pm (1 \pm 0.4)$	< 2

(16), (35), and (37). The results are summarized in Table I. There is no such difficulty for samples with $c < c_2$ since there is no bulk component. The $c_I = 0.004$ (Fig. 11) experimental line shapes clearly reflect a biaxial nature, in particular, the $\theta = \pi/2$ spectra with $2\Delta \nu_{II}/\Delta \nu_I > -1$. To verify if this is a reflection of intrinsic biaxiality η as compared to a diffusion-induced effective biaxiality η_D^{eff} , using Eq. (28) we simulated the angular patterns. The optimal parameters are shown in Table I. There appears to be a better agreement with fits where $D_S \neq 0$, $\eta = 0$, than with those where $D_S = 0$, $\eta \neq 0$ or $D_S \neq 0$, $\eta \neq 0$, as evident from Fig. 11. Additional evidence that supports a diffusion-induced biaxiality comes from the fact that $T_2(\theta = \pi/2)$ is about seven times shorter than $T_2(\theta = 0)$ (see also discussion at the end of Sec. V). That the experimentally determined diffusion constants are close to those found in bulk LC likely indicates that cooperative effects occur in our 2D molecular films.

The $c_{II} = 0.005$ (Fig. 12) system exhibits a small or vanishing biaxiality and/or diffusion rate (Table I). Its larger doublet splitting $\Delta \nu_S$ (as compared with the $c_I = 0.004$ sample) reflects a higher area per molecule A . It is plausible to assume that by increasing A from the saturated value $A(Q_{\text{sat}})$ the molecular cooperative behavior is reduced, resulting in a decrease of the diffusion rate, possibly with a $D_S(A \rightarrow \infty) \rightarrow 0$ limit. The understanding of the spectral features of the saturated surface deposition in terms of a relatively strong surface diffusion is further supported by analyzing its DNMR line width at $\theta = 0$, $\Delta \nu_0$, vs surface coverage plot (Fig. 13). Within experimental error, $\Delta \nu_0$ is independent of A , even for $A < A_2$ where the doublet splitting $\Delta \nu_S$ is strongly A dependent (Fig. 8). If the molecules were frozen and thus not allowed to diffuse, the local value of A would certainly vary over the surface. For $A > A_2$, inhomogeneities in A would give rise to a distribution in $\Delta \nu_S$ which would in turn yield an increase in $\Delta \nu_0$. Since the latter is not observed, we conclude that it is the molecular surface diffusion that renders the area per molecule A homogeneous. All molecules “see” each other very well and consequently one is dealing with a 2D gas, or possibly with a more organized, liquidlike state.

D. Temperature dependencies

Our conclusions regarding the molecular configuration of the surface deposition and for that matter, its existence in itself, also raise a question about the thermodynamic character of such a state. Specifically, are there any anomalies in the temperature dependence of the spectral doublet associated with the surface deposition? An observation of this kind would indicate that the system may evolve from the 2D gas

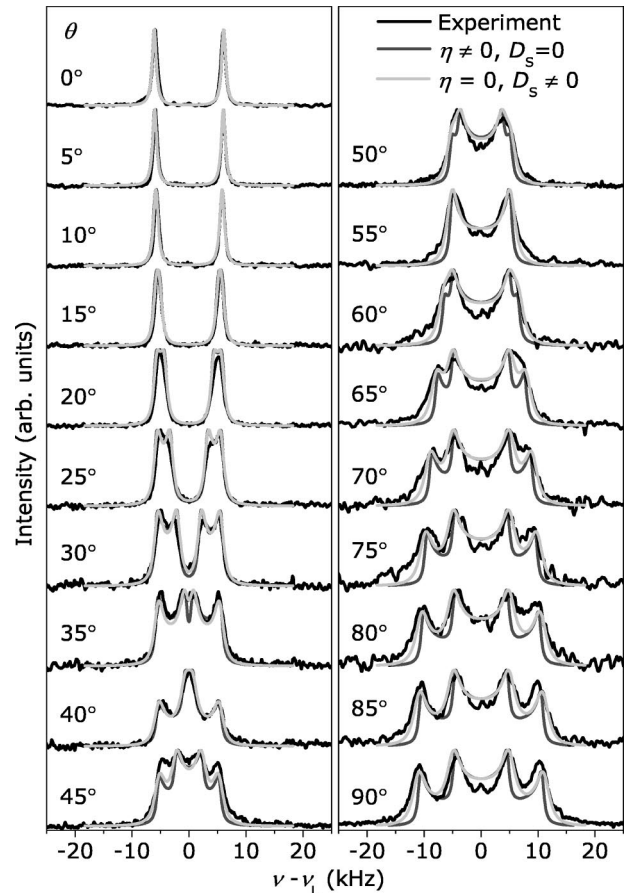


FIG. 11. Experimental and theoretical angular dependencies of the DNMR line shape in the $c_I = 0.004$ system at T_{room} .

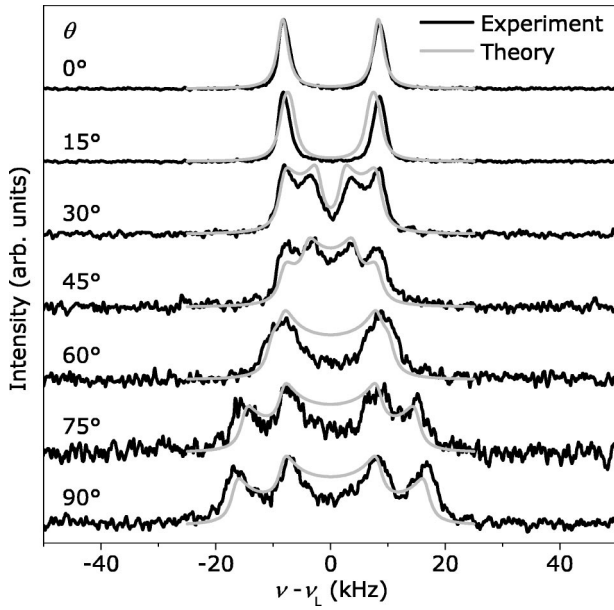


FIG. 12. Experimental and theoretical ($\eta=0$, $D_S \neq 0$) angular dependencies of the DNMR line shape in the $c_{II}=0.005$ system at T_{room} .

class into a 2D liquid collective state class. In order to ascertain this we have measured the temperature dependence of $\Delta\nu_S$ for the $c_I=0.015$, 0.004, and $c_{II}=0.2$, 0.1, 0.05, 0.025, and 0.005 samples (see Fig. 14). For all cases, there is a weak monotonic increase with decreasing temperature. Below $T \approx 270$ K, the approximate temperature at which bulk 5CB crystallizes, the NMR signal was no longer detected. Cooling towards this temperature, the $\Delta\nu_0$ increases dramatically (Fig. 15). Then, the similarity between the bulk 5CB freezing behavior with that of the surface layer again suggests that in the film we are dealing with a collective state. We do note, however, that at high temperatures, a transition of the surface deposition into the isotropic state was not detected in measurements up to 450 K, the highest temperature accessible with our NMR apparatus.

E. Homogeneity and sample stability

The surface deposition doublet at $\theta=0$ consists of rather sharp lines; $\Delta\nu_0(c_{II}=0.001)$ is roughly 10 times smaller than the splitting $\Delta\nu_S$. This indicates that the orientational order is homogeneous, i.e., the respective order parameters Q

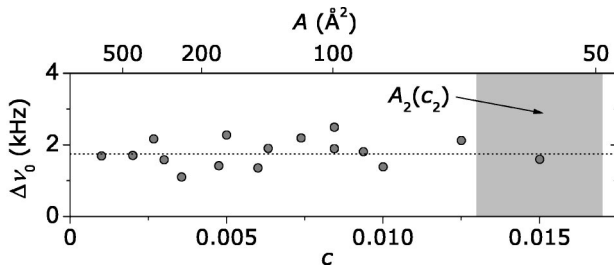


FIG. 13. 5CB surface deposition DNMR doublet linewidth at $\theta=0$ vs surface coverage at T_{room} .

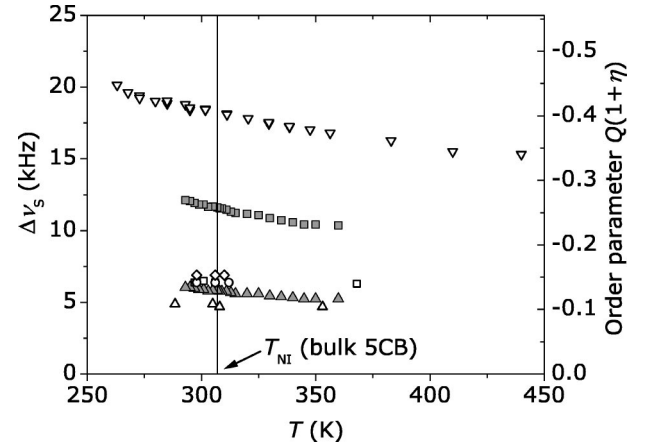


FIG. 14. Temperature dependence of the surface deposition DNMR doublet splitting for the samples with filling factors $c_I=0.015$ (full triangles), $c_I=0.004$ (full squares), $c_{II}=0.2$ (open triangles), $c_{II}=0.1$ (open squares), $c_{II}=0.05$ (open circles), $c_{II}=0.025$ (open diamonds), and $c_{II}=0.005$ (open up triangles).

and η are constant over the cavity surface. Indeed, we assumed this fact earlier to derive the theoretical line shape.

With regards to reproducibility, there is a small discrepancy in results obtained with batch I compared to those obtained with batch II. This is noticeable in the $\Delta\nu_S$ dependence on coverage c for the two batches (Fig. 8) and from Fig. 14 where the $c_I=0.004$ data fall below those for the $c_{II}=0.005$ over the full temperature range. This effect is not surprising since it is quite reasonable to assume that the properties of the molecular depositions may depend on the deposition's preparation process, the liquid crystal batch, and/or on the substrate batch. For instance, due to the existing pore size distribution, departures of the pore radii from its nominal value r_0 could yield [cf. Eq. (1)] such differences.

Finally, DNMR line shapes were measured exclusively with the samples sealed into glass tubes at room temperature and a relative humidity of about 60%. With unsealed samples, fitted into the oxygen and water-vapor poor atmosphere of the vaporized liquid nitrogen used to control the temperature of the continuous flow cryostat housing the NMR magnet, the sharp doublets at $\theta=0$ would rapidly (within 10 min) decay into a broad, powderlike spectra. As already known from other investigations of liquid crystal layers, controlled atmosphere is a crucial factor; when vapor is introduced in the system, as it diffuses through the thin

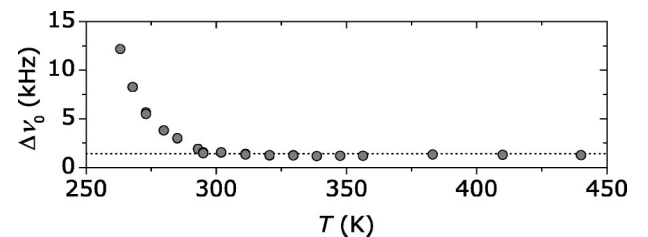


FIG. 15. Temperature dependence of the $c_I=0.005$ 5CB molecular deposition DNMR doublet linewidth at $\theta=0$.

liquid crystal layer it can trigger a hydrogen-bonding controlled anchoring transition [37].

VII. CONCLUSIONS

We have shown that controlled molecular-size effective thickness LC surface depositions can be formed in the cylindrical cavities of the Anopore membranes. We have applied DNMR spectroscopy that allowed us to accurately characterize their physical properties. In addition to a bulklike component with parallel axial director configuration that is compatible with that found when Anopore are completely filled, a second, surface-controlled component of planar radial director configuration is present in partially filled Anopores with sufficiently low area per molecule value A . This component is identified as a thin molecular deposition of mesogenic molecules. The interplay between the bulk and the deposition is characterized by a typical dewetting scenario. The surface equivalents of the bulk order parameters components, namely, the surface orientational order Q and the surface biaxiality η , are uniform over the surface and weakly dependent on temperature. Below a critical surface coverage c , Q strongly increases with decreasing c , reaching $Q \approx$

$-1/2$ in the $c \rightarrow 0$ (or equivalently, $A \rightarrow \infty$) limit, demonstrating than in a highly diluted molecular deposition the molecules lie flat on the surface. A model that incorporates a motionally induced biaxiality provides the best fits to the data; there is a fast surface diffusion that is of the same order of magnitude as in the bulk LC phase. The surface phase has a 2D gas character. Some indicators, although not totally conclusive, of a collective 2D liquid character are also found. Additional DNMR studies in these nematic systems as well as with smectic liquid crystals to investigate their growth at the surface would be illuminating. Studies with different and decreasing pore sizes to quantify curvature effects on the deposition's behavior, as well as probing these systems with different experimental techniques would be important.

ACKNOWLEDGMENTS

This work was supported by Grants No. NSF-ALCOM 89-20147 and No. NSF-INT (USA-Slovenia) 98-15313. We are particularly grateful to Mary Neubert and co-workers for providing us with the deuterated materials. We also thank Dr. Igor Muševič and Dr. Irena Drevenšek for many illuminating conversations.

-
- [1] F. M. Gasparini and I. Rhee, in *Progress in Low Temperature Physics*, edited by D. F. Brewer (North-Holland, Amsterdam, 1992), Vol. XIII, Chap. 1.
- [2] L.M. Steele, C.J. Yeager, and D. Finotello, *Phys. Rev. Lett.* **71**, 3673 (1993).
- [3] D.J. Bishop and J.D. Reppy, *Phys. Rev. Lett.* **40**, 1727 (1978).
- [4] D. Finotello and F.M. Gasparini, *Phys. Rev. Lett.* **55**, 2156 (1985).
- [5] F. Vandenbrouck, M.P. Valignat, and A.M. Cazabat, *Phys. Rev. Lett.* **82**, 2693 (1999).
- [6] P. Zihlerl, R. Podgornik, and S. Žumer, *Phys. Rev. Lett.* **84**, 1228 (2000); **82**, 1189 (1999).
- [7] M.P. Valignat, S. Villette, J. Li, R. Barberi, R. Bartolino, E. Dubois-Violette, and A.M. Cazabat, *Phys. Rev. Lett.* **77**, 1994 (1996).
- [8] B. Zalar, S. Žumer, and D. Finotello, *Phys. Rev. Lett.* **84**, 4866 (2000).
- [9] I. Drevenšek *et al.* (unpublished).
- [10] Y. Iwakabe, M. Hara, K. Kondo, K. Tochigi, A. Mukoh, A. Yamada, A.F. Garito, and H. Sasabe, *J. Acoust. Soc. Jpn.* **30**, 2542 (1991).
- [11] J. Xue, C.S. Jung, and M.W. Kim, *Phys. Rev. Lett.* **69**, 474 (1992).
- [12] A.J. Leadbetter, R.M. Richardson, and C.N. Colling, *J. Phys. (Paris), Colloq.* **36**, C1-37 (1975).
- [13] A. Sugimura, M. Iwamoto, O.Y. ZhongCan, *Mol. Cryst. Liq. Cryst. Sci. Technol., Sect. A* **263**, 429 (1995).
- [14] G.P. Crawford, R.J. Ondris-Crawford, J.W. Doane, and S. Žumer, *Phys. Rev. E* **53**, 3647 (1996), and references therein.
- [15] G.P. Crawford, R. Ondris-Crawford, S. Žumer, and J.W. Doane, *Phys. Rev. Lett.* **70**, 1838 (1993).
- [16] T. Moses and Y.R. Shen, *Phys. Rev. Lett.* **67**, 2033 (1991).
- [17] A. Rapini and M. Papoular, *J. Phys. (Paris), Colloq.* **30**, C4-45 (1969).
- [18] M. Vilfan, N. Vrbancič-Kopač, B. Zalar, S. Žumer, and G.P. Crawford, *Phys. Rev. E* **59**, R4754 (1999).
- [19] S. Faetti, M. Gatti, V. Palleschi, and T.J. Sluckin, *Phys. Rev. Lett.* **55**, 1681 (1985).
- [20] S. Kralj, G. Lahajnar, A. Zidanšek, N. Vrbancič-Kopač, M. Vilfan, R. Blinc, and M. Kosec, *Phys. Rev. E* **48**, 340 (1993).
- [21] *Liquid Crystals in Complex Geometries Formed by Polymer and Porous Network*, edited by G.P. Crawford and S. Žumer (Taylor & Francis, London, 1996).
- [22] G.P. Crawford, D.K. Yang, S. Žumer, D. Finotello, and J.W. Doane, *Phys. Rev. Lett.* **66**, 723 (1991).
- [23] J. Fukusawa, C.D. Poon, and E.T. Samulski, *Langmuir* **7**, 1727 (1991).
- [24] R. Seidin, R.M. Hornreich, and D.W. Allender, *Phys. Rev. E* **55**, 4302 (1997).
- [25] J. Struppe and F. Noack, *Liq. Cryst.* **20**, 595 (1996).
- [26] M. Vilfan, G. Lahajnar, I. Zupančič, S. Žumer, R. Blinc, G.P. Crawford, and J.W. Doane, *J. Chem. Phys.* **103**, 8726 (1995).
- [27] B. Jérôme, *Rep. Prog. Phys.* **54**, 391 (1991).
- [28] J.C. Rowell, W.D. Phillips, L.R. Melby, and M. Panar, *J. Chem. Phys.* **43**, 3442 (1965).
- [29] J.W. Emsley, G.R. Luckhurst, and C.P. Stockley, *Mol. Phys.* **44**, 565 (1981).
- [30] P.G. de Gennes and J. Prost, *The Physics of Liquid Crystals* (Oxford University Press, Oxford, 1993).
- [31] J.W. Doane, in *Magnetic Resonance of Phase Transitions*, edited by F.J. Owens, C.P. Poole, and H.A. Farach (Academic Press, New York, 1979).
- [32] E.W. Weisstein, *CRC Concise Encyclopaedia of Mathematics* (Springer-Verlag, Berlin, 1999).

- [33] M. Vilfan, T. Apih, A. Gregorovič, B. Zalar, G. Lahajnar, S. Žumer, G. Hinze, R. Böhmer, and G. Althoff, *Magn. Reson. Imaging* **19**, 433 (2001).
- [34] A. Abragam, *Principles of Nuclear Magnetism* (Oxford University Press, Oxford, 1961).
- [35] G. Chidichimo, Z. Yaniv, N.A.P. Vaz, and J.W. Doane, *Phys. Rev. A* **25**, 1077 (1982).
- [36] Z. Yaniv, N.A.P. Vaz, G. Chidichimo, and J.W. Doane, *Phys. Rev. Lett.* **47**, 46 (1981).
- [37] J. Bechhoefer, B. Jerome, and P. Pieranski, *Phys. Rev. A* **41**, 3187 (1990).